



UNIVERSITY OF LEEDS

This is a repository copy of *Shallow water methane-derived authigenic carbonate mounds at the Codling Fault Zone, western Irish Sea.*

White Rose Research Online URL for this paper:  
<http://eprints.whiterose.ac.uk/82704/>

Version: Accepted Version

---

**Article:**

O'Reilly, SS, Hryniewicz, K, Little, CTS et al. (6 more authors) (2014) Shallow water methane-derived authigenic carbonate mounds at the Codling Fault Zone, western Irish Sea. *Marine Geology*, 357. 139 - 150. ISSN 0025-3227

<https://doi.org/10.1016/j.margeo.2014.08.007>

---

**Reuse**

Unless indicated otherwise, fulltext items are protected by copyright with all rights reserved. The copyright exception in section 29 of the Copyright, Designs and Patents Act 1988 allows the making of a single copy solely for the purpose of non-commercial research or private study within the limits of fair dealing. The publisher or other rights-holder may allow further reproduction and re-use of this version - refer to the White Rose Research Online record for this item. Where records identify the publisher as the copyright holder, users can verify any specific terms of use on the publisher's website.

**Takedown**

If you consider content in White Rose Research Online to be in breach of UK law, please notify us by emailing [eprints@whiterose.ac.uk](mailto:eprints@whiterose.ac.uk) including the URL of the record and the reason for the withdrawal request.



[eprints@whiterose.ac.uk](mailto:eprints@whiterose.ac.uk)  
<https://eprints.whiterose.ac.uk/>

1 **Shallow water methane-derived authigenic carbonate mounds at the**  
2 **Codling Fault Zone, western Irish Sea**

3

4 Shane S. O'Reilly<sup>a</sup>, Krzysztof Hryniewicz<sup>b</sup>, Crispin T.S. Little<sup>c</sup>, Xavier  
5 Monteys<sup>d</sup>, Michal T. Szpak<sup>a</sup>, Brian T. Murphy<sup>a</sup>, Sean F. Jordan<sup>a</sup>,  
6 Christopher C.R. Allen<sup>e</sup>, Brian P. Kelleher<sup>a\*</sup>.

7

8 <sup>a</sup> School of Chemical Sciences, Dublin City University, Glasnevin, Dublin 9, Ireland.

9 <sup>b</sup>Natural History Museum, University of Oslo, 1172 Blindern, 0318 Oslo, Norway.

10 <sup>c</sup>School of Earth and Environment, University of Leeds, Leeds LS2 9JT, United  
11 Kingdom.

12 <sup>d</sup>Geological Survey of Ireland, Beggars Bush, Haddington Road, Dublin 4, Ireland.

13 <sup>e</sup>*School of Biological Sciences, Queen's University Belfast, University Road, Belfast*  
14 *BT7 1NN, United Kingdom.*

15 \* Corresponding author – Brian P Kelleher

16 School of Chemical Sciences, Dublin City University, Glasnevin, Dublin 9, Ireland.

17 [brian.kelleher@dcu.ie](mailto:brian.kelleher@dcu.ie)

18 Tel: 00353 1 7005134

19

20

21

22

23

24 **Abstract**

25 Methane-derived authigenic carbonate (MDAC) mound features at the Codling Fault  
26 Zone (CFZ), located in shallow waters (50 to 120 m) of the western Irish Sea were  
27 investigated and provide a comparison to deep sea MDAC settings. Carbonates  
28 consisted of aragonite as the major mineral phase, with  $\delta^{13}\text{C}$  values as low as -50‰.  
29 These isotope signatures, together with the co-precipitation of framboidal pyrite  
30 confirm that anaerobic oxidation of methane (AOM) is an important process  
31 mediating methane release to the water column and the atmosphere in this region. The  
32  $^{13}\text{C}$  depletion of bulk carbonate and sampled gas (-70‰) suggests a biogenic source,  
33 but significant mixing of thermogenic gas and depletion of the original isotope  
34 signature cannot be ruled out. Active seepage was recorded from one mound and  
35 together with extensive areas of reduced sediment, confirms that seepage is ongoing.  
36 The mounds appear to be composed of stacked pavements that are largely covered by  
37 sand and extensively eroded. The CFZ mounds are colonized by abundant Sabellaria  
38 polychaetes and possible Nemertesia hydroids, which benefit indirectly from available  
39 hard substrate. In contrast to deep sea MDAC settings where seep-related macrofauna  
40 are common reported, seep-specialist fauna appear to be lacking at the CFZ. In  
41 addition, unlike MDAC in deep waters where organic carbon input from  
42 photosynthesis is limited, lipid biomarkers and isotope signatures related to marine  
43 planktonic production (e.g. sterols, alkanols) were most abundant. Evidence for  
44 microbes involved in AOM was limited from samples taken; possibly due to this  
45 dilution effect from organic matter derived from the photic zone, and will require  
46 further investigation.

47

48 Keywords: Methane-derived authigenic carbonate, gas seepage, Codling Fault, Irish  
49 Sea

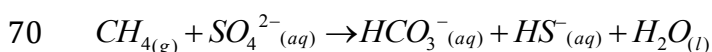
50 Abbreviations: Anaerobic oxidation of methane (AOM), Codling Fault Zone (CFZ),  
51 Dimethyl disulfide (DMDS), Energy-dispersive spectroscopy (EDS), Fatty acid  
52 methyl ester (FAME), Methane-derived authigenic carbonate (MDAC), Mono-alkyl  
53 glycerol ethers (MAGE), Scanning electron microscopy (SEM), X-Ray diffraction  
54 (XRD).

55

## 56 **1. Introduction**

57 Methane is an important trace gas in the atmosphere and a potent greenhouse gas  
58 (Svensen et al., 2004; Forster et al., 2007). Seepage of methane from the ocean's  
59 seafloor is of global occurrence, yet one that is poorly quantified and understood  
60 (Fleischer et al., 2001; Knittel and Boetius, 2009). One result of seabed seepage is the  
61 formation of distinctive seafloor structures, such as pockmarks, mud diapirs, mud  
62 volcanoes and methane-derived authigenic carbonates (MDAC). MDAC, which may  
63 form pavements or mound structures, are produced as a direct result of methane  
64 supply from the subsurface to shallow sediment and the sediment-water interface (e.g.  
65 Bohrmann et al., 1998; Aloisi et al., 2000; Greinert et al., 2002; Bayon et al., 2009).  
66 There, methane is utilized by a consortium of methane-oxidizing archaea and sulfate-  
67 reducing bacteria in the anaerobic oxidation of methane (AOM) reaction (Hinrichs et  
68 al., 1999; Boetius et al., 2000; Reitner et al., 2005) according to Equation 1:

69



71 Eqn. 1

72 The reaction is maintained in expense of marine sulfate dissolved in pore waters  
73 (Boetius et al., 2000; Tsunogai et al., 2002; Niemann et al., 2005). If the supply of  
74 methane is sufficient, AOM leads to supersaturation of pore fluids with respect to  
75  $\text{HCO}_3^-$  and in result facilitates the formation of MDAC (Hovland et al., 1987; Stakes  
76 et al., 1999; Greinert et al., 2001; Mazzini et al., 2005; Naehr et al., 2007; Paull et al.,  
77 2007; Feng et al., 2008).  $\text{HS}^-$  is typically precipitated as pyrite ( $\text{FeS}_2$ ) on reaction with  
78 Fe in pore fluids (e.g. Peckmann et al., 2001; Pechmann and Thiel, 2004). Recent  
79 evidence indicates that the bacterial partners involved in AOM may be more diverse  
80 than previously thought (Beal et al., 2009) and that ANME may be able to perform  
81 AOM without bacterial partners (Milucka et al., 2012). AOM is responsible for the  
82 oxidation of possibly 90% of marine methane (Knittel and Boetius, 2009) and hence  
83 AOM and MDAC formation are important for regulation of ocean to atmosphere  
84 carbon fluxes (e.g. Aloisi et al., 2002). Methane consumption via AOM is estimated  
85 to be in the range of 5 to 20% of net modern atmospheric methane flux (20 to 100  
86  $\times 10^{12} \text{ g a}^{-1}$ ) (Valentine and Reeburgh, 2000). Many sites of active methane seepage  
87 have been shown to support unique macro- and micro-faunal biodiversity (e.g. Dando  
88 et al., 1991; Jensen et al., 1992; Sibuet and Olu, 1998; Van Dover et al., 2003; Olu-Le  
89 Roy et al., 2004). In addition, gas seepage features are important in relation to marine  
90 industrial and petroleum safety (Hovland et al., 2002), and also in petroleum and gas  
91 prospecting (Judd and Hovland, 2007).

92 Most cold seeps with extensive MDAC have been reported from the deep sea  
93 (e.g. Ritger et al., 1987; von Rad et al., 1996; Chen et al., 2005; Feng et al., 2010;  
94 Haas et al., 2010; Crémière et al., 2012; Magalhães et al., 2012), but reports of  
95 extensive MDAC occurrence within the photic zone (0 to ~200 m water depth) are  
96 also common. Shallow cold seep settings with extensive MDAC occurrence include

97 the Coal Oil Point Seep field, off Santa Barbara (Kinnaman et al., 2010), St.  
98 Lawrence Estuary, Canada (Lavoie et al., 2010), Monterey Bay (Stakes et al., 1999),  
99 the Kattegat (Jørgensen, 1989; Jensen et al., 1992), the Adriatic (Capozzi et al., 2012),  
100 the northwestern Black Sea (Peckmann et al., 2001), the North Sea (Judd and  
101 Hovland, 2007), and recently the Texel 11 and Holden's Reef sites in the Irish Sea  
102 (Judd et al., 2007). Shallow water seep assemblages contain lower percentage of seep  
103 specialists than deep water sites and are instead dominated by background fauna  
104 (Levin et al., 2000; Rathburn et al., 2000; Dando, 2010), probably due to the increased  
105 influence and input of photosynthetic carbon in shallow depths (Levin, 2005). In  
106 contrast to deep water sites, which can support abundant assemblages of seep-  
107 restricted chemosymbiotic macrofauna, most symbiont-bearing taxa found in shallow  
108 water sites are shared with non-seep reducing environments (Sahling et al., 2003).

109         The Irish Sea contains extensive areas of shallow gas accumulation, as well as  
110 numerous occurrences of seabed features associated with gas migration (Croker,  
111 1995; Croker et al., 2005). Twenty-three mounds features have recently been  
112 identified along the Codling Fault Zone (CFZ) in the east perimeter of the Kish Bank  
113 Basin in the western Irish Sea (Fig. 1) (Croker et al., 2002; 2005; Judd et al., 2007).  
114 Based on extensive mapping and ground-truthing, Croker et al. (2002; 2005)  
115 concluded that the mounds at the CFZ were MDAC and that this site is the most  
116 active site of gas seepage in the Irish designated zone of the Irish Sea. A number of  
117 the CFZ mounds were investigated in 2010 during INFOMAR (Integrated Mapping  
118 for the Sustainable Development of Ireland's Marine Re) survey CV10\_28. The  
119 purpose of this study was to further ground-truth the CFZ carbonate mound features,  
120 to provide further mineralogical, geochemical and isotopic evidence that these  
121 features are formed by AOM, to provide evidence of current active seepage, and

122 finally to compare this site to other extensive MDAC occurrences in shallow and deep  
123 sea settings.

124

## 125 **2. Environmental and geological setting**

126 The western Irish Sea (west of 5°20') encompasses two Mesozoic sedimentary basins,  
127 namely the Kish Bank Basin and the southwest section of the Central Irish Basin, and  
128 is primarily underlain with Permian and Carboniferous rocks. Quaternary deposits up  
129 to 150 m thick occur, but are laterally discontinuous, locally revealing exposed  
130 bedrock (Croker et al., 2005). The northwest Irish Sea (north of 53°30') is  
131 characterised by relatively weak hydrodynamic conditions, resulting in the seabed  
132 being dominated by fine silty mud. This is in contrast to the southern region where the  
133 CFZ is located. This region is subject to comparatively high-energy currents and is  
134 characterised by gravelly sands and cobbles, and high-energy bedforms such as sand  
135 streaks, sand ribbons, gravel furrows and sand waves (Croker et al., 2005). The water  
136 depth here is 50 to 60 m at the west of the fault and 80 to 120 m to its east. The CFZ  
137 is a major northwest-southeast trending strike-slip fault and consists of a complex  
138 fault zone several kilometers wide (Jackson et al., 1995). Croker et al. (2005) divided  
139 the fault into three zones: the northern muddy zone containing the Lambay Deep and  
140 its associated mud diapir; the central sandy zone characterised by large sand waves;  
141 and the southern zone characterised by current-swept seabed and patches of coarse  
142 sediments. The CFZ mounds have been identified in the central zone and have a relief  
143 of 5 to 10 m. They are typically greater than 250 m in length and over 80 m in width.  
144 For a detailed discussion of the setting and geology of the study area see Dobson and  
145 Whittington (1979) and Jackson et al. (1995).

146

### 147 **3. Materials and Methods**

148 Bathymetry data was collected from the CFZ from 2001 to 2002 during Celtic  
149 Voyager survey (Croker and O'Loughlin, 2001) and available through the INFOMAR  
150 program. Data was collected using a Kongsberg Simrad EM1002 multibeam  
151 echosounder (for details, see Croker and O'Loughlin, 2001). During survey CV10\_28  
152 water column echofacies were monitored using a Kongsberg Simrad EA400 single  
153 beam echosounder operated at 38 kHz. A Kongsberg Simrad OE14-208 underwater  
154 towed video system, housed in a Seatronics frame was used to obtain video and image  
155 stills of the mound features and surrounding seabed. Sediment sampling was  
156 conducted using Shipek and Van Veen grabs. Hardground material was retrieved from  
157 three stations, G103, G107 and G109, as shown in Fig. 1. Hardgrounds at each station  
158 were combined as one sample per station. Details for the sampling stations are given  
159 in Table 1. Samples for geochemical analysis were stored at  $-20^{\circ}\text{C}$  onboard and at  $-$   
160  $80^{\circ}\text{C}$  in the laboratory. The redox potential ( $E_h$ ) of sampled sediments was assessed  
161 using an ORP ProcessProbe Ag/Cl redox probe (Bradley James Corp., Bedford, UK).

162 Unoriented rock slabs from G109 were cut using a diamond rock cutter and  
163 polished with sandpaper. Some polished slabs were used to prepare uncovered  
164 petrographic thin sections of standard size (48 mm x 28mm). Optical petrographic  
165 microscopy was performed using Leica DC 300 digital camera mounted on Leica  
166 DMLP microscope under the magnifications of 2.5, 5, 10, 20 and 40x. Relative  
167 abundances of grains in relation to pore space were estimated using comparison charts  
168 (Bacelle and Bosellini, 1965). Finely ground, hand-drilled carbonate samples from  
169 G109 were analysed for stable  $\delta^{13}\text{C}$  and  $\delta^{18}\text{O}$  isotope ratios using Finnigan MAT 251  
170 and MAT 253 mass spectrometers coupled to automated Kiel devices.  $\delta^{13}\text{C}$   
171 measurement of methane from sediment samples in headspace vials from a core

172 catcher was performed on a Finnegan MAT DeltaPlus irMS after conversion to CO<sub>2</sub>  
173 (Organic Mass Spectrometry Facility, Woods Hole Oceanographic Institute). Isotope  
174 results are measured in relation to standard Vienna Pee Dee Belemnite (VPDB), with  
175 long-term analytical precision around 0.05% for  $\delta^{13}\text{C}$  and 0.1% for  $\delta^{18}\text{O}$ .

176 Standard X-ray diffraction (XRD) in order to identify primary minerals was  
177 performed on mortar-ground samples using Siemens D5005 powder X-ray  
178 diffractometer. Scanning electron microscopy (SEM) was performed using a Hitachi  
179 S3400-N scanning electron microscopy operated at an accelerating voltage of 15.0 kV  
180 and a working distance of 10 cm. Elemental composition was assessed using an INCA  
181 Energy energy dispersive spectrometer (Oxford Instruments, UK) fitted to a Hitachi  
182 SU-70 SEM. SEM-energy dispersive spectroscopy (EDS) was performed at an  
183 accelerating voltage of 15.0 kV and a working distance of 1.6 cm. Elemental data was  
184 processed with the INCA suite software.

185 Sampled hardgrounds were acid solubilised (2 M HCl) and extracted  
186 according to Niemann et al. (2005) by ultrasonication-assisted extraction with the  
187 following solvent regime: 2:1 (v/v) methanol/DCM (x2), 1:2 (v/v) methanol/DCM  
188 (x2) and DCM (x2). Total lipid extracts were saponified with 6% KOH in methanol  
189 (80°C for 3 hr) and neutral lipids and fatty acids (at ~ pH 1) were recovered by liquid-  
190 liquid extraction (x3) with 9:1 (v/v) hexane/diethyl ether. Neutral lipids were  
191 derivatised with N,O- bis(trimethylsilyl) trifluoroacetamide/pyridine (9:1, v/v), while  
192 fatty acids were methylated with 14% BF<sub>3</sub> in methanol at 70°C for 1 hr. Fatty acid  
193 methyl ester (FAME) monounsaturations position was confirmed by formation of  
194 dimethyl disulfide (DMDS) adducts as outlined by Nichols et al. (1986). Analysis was  
195 performed on an Agilent 6890N gas chromatograph interfaced with an Agilent 5975C  
196 mass selective detector according to O'Reilly et al. (2012; 2014). The column

197 temperature program was as follows: 65°C injection and hold for 2 min, ramp at 6°C  
198 min<sup>-1</sup> to 300°C, followed by isothermal hold at 300°C for 20 min. Quantification was  
199 performed using 5- $\alpha$ -cholestane internal standard. Samples were analysed in duplicate  
200 by continuous flow isotope ratio mass spectrometry (IsoPrime) according to O'Reilly  
201 et al. (2012; 2014), and using identical GC conditions as above.  $\delta^{13}\text{C}$  values were  
202 calibrated against a stable isotope reference standard comprising a mixture of 15 n-  
203 alkanes (Mixture B2, Indiana University). Average  $\delta^{13}\text{C}$  values are reported after  
204 correction for addition of derivative groups where necessary. Fatty acid nomenclature  
205 is according to xC<sub>y<sub>o</sub>z</sub>, where x refers to the number of carbon atoms present, y refers to  
206 the number of double bonds on the carbon chain and z refers to the position of the first  
207 double bond from the methyl end.

208

## 209 **4. Results**

### 210 **4.1 Underwater towed video, sampling and single beam echosounder**

211 Collected video and image stills of the seabed at and in the vicinity of the mound  
212 targets are presented in Fig. 2. The sediment type was primarily fine- to coarse-  
213 grained sand, and there was widespread occurrence of exposed and semi-exposed  
214 hardgrounds on the seabed in the vicinity of target sites (Fig. 2A and B). These  
215 features appeared to be largely buried by sand. Fig. 2C shows an underwater still  
216 image of an area of exposed stacked pavement. This shows large 10 to 20 cm thick  
217 slabs and likely represents the characteristic morphology of the CFZ mounds. Patches  
218 of black, apparently reduced seabed several centimetres across were also recorded  
219 (Fig. 2D and F) during video surveying. A high density of asterozoans (likely  
220 ophiuroids) was observed in the vicinity of the mounds (not shown). In addition,  
221 possible hydroids colonising hardgrounds were also recorded (Fig. 2D to F).

222 Grab sampling of stations G103, G107 and G109 retrieved hardground  
223 material (hereafter referred to as G103, G107 or G109) and some black sediment.  
224 Sampled black surface sediments (Fig. 2G and I) were confirmed to be reducing,  
225 exhibiting  $E_h$  readings as low as -177 mV. Colonising hydroids were also retrieved,  
226 still physically attached to sampled hardgrounds (Fig. 2G and H). These possibly  
227 belong to the genus *Nemertesia*, which have been found at the Texel carbonate mound  
228 sites ( $\sim 53^{\circ}27'N$ ,  $5^{\circ}12'W$ ) in the mid-Irish Sea (Whomersley et al., 2010). Grab  
229 sampling stations G103, G107 and G109 contained cemented tube worms (Fig. 2G).  
230 These are likely to have been formed by sedentary sabellarid polychaetes, possibly  
231 *Sabellaria spinulosa*, which are abundant at other hard grounds in the Irish Sea  
232 (Whomersley et al., 2010).

233 Single beam echosounder transects across one of the mounds (Fig. 1B) yielded  
234 characteristic acoustic echofacies in the water column. These appear as a rising  
235 vertical plume from close to the apex of the mound (Fig. 3). This acoustic signal is  
236 either caused by fish shoals or gas bubbles. However, fish shoals would normally  
237 display a broader more horizontal profile (Judd and Hovland, 2007), and by virtue of  
238 the source and vertical profiles this is very likely a gas plume emanating from the  
239 mound. The plume was detected rising a number of metres into the water column and  
240 the profile indicates at least moderate seepage is taking place at the CFZ.

241

#### 242 **4.2 Mineralogy, petrographic analysis and stable isotope analysis**

243 Sub-samples from G103, G107 and G109 were also analysed using SEM-EDS  
244 analysis (Fig. 4). EDS spectra were dominated by calcium, silica, carbon and oxygen,  
245 confirming that the hard grounds are composed of carbonate and carbonate-cemented  
246 quartz grains (Fig. 4A and B). Individual quartz grains cemented by this carbonate are

247 shown in Fig. 4C. Sulfur was also identified from EDS spectra, in particular for G109  
248 (Fig. 4B). SEM micrographs highlighted the occurrence of amorphous to well-  
249 developed framboidal pyrite as the source of this sulfur (Fig. 4D and E). Based on the  
250 crystal shapes observed in SEM, the carbonate appears to a primarily acicular  
251 aragonite. Further petrographic analysis (Fig. 5, thin section PMO 217.327) and XRD  
252 (Fig. 6) of G109 confirmed that quartz and aragonite are the major mineral  
253 constituents of the rock. The rock can be subdivided into two main components. A  
254 detrital component is composed mostly of quartz sand (Fig. 5A), with small  
255 admixtures of other grains, such as mudstone lithoclasts, glaucony grains (Fig. 5B)  
256 and bioclasts. Among the bioclasts, possible red algae (Fig. 5B), echinoderms (Fig.  
257 5B), bivalve fragments (Fig. 5C), balanid barnacles (Fig. 5D), foraminifera and  
258 gastropods (Fig. 5E and F) have been identified. This component can be linked with  
259 quartz and magnesian calcite, as identified by XRD (Fig. 6). The total grain fabric  
260 constitutes around 60% of the rock volume. Pore space partially occluded by the  
261 authigenic component occupies the remaining 40% of rock volume. The authigenic  
262 component is composed almost solely of aragonite (Fig. 6). It is represented by the  
263 microcrystalline variety, lining the surface of some of the grains and occasionally  
264 forming clothed microfabrics, followed by more abundant acicular crystals cementing  
265 the pore space (Fig. 5).

266 Carbonate stable isotope data have been obtained from sites G107 and G109.  
267 The  $\delta^{13}\text{C}$  value from a single sample from site G107 are shown in Table 1. Samples  
268 from site G109 are presented in Table 1 (range) and Table 2 (all data points). Site  
269 G107 shows depleted  $\delta^{13}\text{C}$  carbon (-36.97‰). Site G109 shows depleted  $\delta^{13}\text{C}$  values  
270 between -48.97‰ and -53.71‰ (Fig. 7).  $\delta^{18}\text{O}$  varied between -0.80‰ and 2.58‰

271 (Fig. 7).  $\delta^{13}\text{C}$  values for methane sampled from surface sand at the CFZ mounds (Lat.  
272  $53^{\circ}20'50''\text{N}$ , Long.  $5^{\circ}39'10''\text{W}$ ) measured  $-70\text{‰}$ .

273

#### 274 **4.3 Lipid biomarkers and compound specific stable carbon isotope analysis**

275 Fatty acids distribution was similar between G103, G107 and G109, whereby a range  
276 of saturated, monounsaturated, polyunsaturated, methyl- and cyclopropyl fatty acids  
277 were observed (Fig. 8A). Fatty acids ranged from  $\text{C}_{12}$  to  $\text{C}_{26}$  homologs.  $\text{C}_{16:0}$  was the  
278 major fatty acid in all samples.  $\text{C}_{14:0}$  and  $\text{C}_{18:0}$  were other major saturated fatty acids.  
279 Monounsaturated  $\text{C}_{16:1\omega7}$  and  $\text{C}_{18:1\omega7}$  were also major fatty acids, followed by the  
280 polyunsaturated fatty acids  $\text{C}_{20:5\omega3}$ ,  $\text{C}_{20:4\omega6}$ ,  $\text{C}_{22:6\omega3}$  and  $\text{C}_{22:5\omega6}$ . Iso and anteiso methyl  
281 branched fatty acids were also abundant and were dominated by odd carbon  $\text{C}_{15}$  and  
282  $\text{C}_{17}$  homologs. These included  $\text{iC}_{15:0}$ ,  $\text{aiC}_{15:0}$ ,  $\text{iC}_{16:0}$ ,  $10\text{MeC}_{16:0}$  and  $\text{iC}_{17:0}$ . The average  
283 ( $n = 2$ ) measured  $\delta^{13}\text{C}$  values for selected lipids from G103, G107 and G109 are given  
284 in Fig. 9. The  $\delta^{13}\text{C}$  measurements for fatty acids ranged from  $-24\text{‰}$  to as low as -  
285  $39\text{‰}$ . A general trend of between  $-25\text{‰}$  to  $-29\text{‰}$  was observed with overall little  
286 variation between samples for each compound. However, the branched fatty acids  
287  $\text{aiC}_{15:0}$ ,  $\text{iC}_{16:0}$ ,  $10\text{MeC}_{16:0}$  and  $\text{C}_{17:1}$  were more depleted (below  $-30\text{‰}$ ) for G109, as  
288 well as with  $\text{iC}_{16:0}$  for G107. Sterols were the major lipid class in the neutral lipid  
289 fractions.  $\text{C}_{27}\Delta^5$  was the major sterol in all samples.  $\text{C}_{26}\Delta^{5,22}$ ,  $\text{C}_{27}\Delta^{5,22}$ ,  $\text{C}_{28}\Delta^{5,22}$ ,  
290  $\text{C}_{29}\Delta^{5,22}$ ,  $\text{C}_{29}\Delta^5$  and  $\text{C}_{29}\Delta^{5,24(28)}$  were also identified.  $\delta^{13}\text{C}$  values were about  $-28\text{‰}$  for  
291 well-resolved major sterols (Fig. 9). Other major lipids included phytol, n-alkanols  
292 ( $\text{C}_{14}$  to  $\text{C}_{26}$ ), a range of mono-alkyl glycerol ethers (MAGE) with n-alkyl chain  
293 lengths from  $\text{C}_{14}$  to  $\text{C}_{20}$ . Pentamethylcosane was identified in G109 in low  
294 abundance, as well as crocetane co-eluting with phytane. Archaeol was tentatively

295 identified in low abundance in G103 and G109 based on the peaks at m/z 130, 278  
296 and 426. The abundance of these lipids was too low to permit  $\delta^{13}\text{C}$  measurement.

297

## 298 **5. Discussion**

299 Methanogenesis in marine sediments can be subdivided into three main stages. The  
300 first stage takes place during shallow burial, when in temperatures lower than 50°C  
301 organic matter is being converted into methane by series of biochemical processes  
302 (Mah et al., 1977). In later burial at 80°C to 120°C, thermal cracking of organic  
303 matter forms gaseous and liquid hydrocarbons, which are further cracked to methane  
304 in when temperatures reach ca. 150°C (Claypool and Kvenvolden, 1983). Each of the  
305 formation stages leaves a characteristic trace in isotopic and chemical composition of  
306 the resulting gas (Schoell, 1988; Whiticar, 1999), which can be used to trace back the  
307 origin of the methane (e.g. Martens et al., 1991; Ivanov et al., 2010). Usually, the  
308 biogenic methane is significantly depleted in the heavy carbon isotope, with  $\delta^{13}\text{C}$   
309 values below -50‰, with thermogenic methane ranging between -50‰ to -30‰  
310 (Sackett, 1978; Peckmann and Thiel, 2004; Judd and Hovland, 2007).

311 Heavily depleted carbon isotope (as low as -53.7‰) data from hardgrounds  
312 sampled at stations G107 and G109 confirm that the CFZ mounds are MDAC, and  
313 support previous work from Croker et al. (2002; 2005). **Along with sites at Texel 11,**  
314 **Holden's Reef (Judd, 2005; Judd et al., 2007), and the mid-Irish Sea (Milodowski et**  
315 **al., 2009), the CFZ mounds are the fourth confirmed occurrence of MDAC in the Irish**  
316 **Sea.** Usually MDAC is less depleted than the parent gas due to mixing with carbon  
317 from other sources, so the exact correlation between carbonate and parent gas is not  
318 straightforward (e.g. Bohrmann et al., 1998; Peckmann et al., 2001; Schmidt et al.,  
319 2002; Peckmann and Thiel, 2004). The amount of mixing is unknown, but seeping

320 methane was likely isotopically lighter than cements (-70‰) and hence possibly of  
321 biogenic origin.

322         The CFZ MDAC samples are enriched in  $^{18}\text{O}$  compared to typical marine  
323 carbonates, which usually range from -10‰ to +2‰ (Nelson and Smith, 1996).  
324 However, these values are in agreement with isotope signatures from MDAC recently  
325 sampled in the mid Irish Sea (Milodowski et al., 2009). The regression line in Fig. 7  
326 for the cluster of data points shows a strong correlation ( $n = 7$ ,  $R^2 = 0.90$ ) and  
327 intersects the x-axis at  $\delta^{13}\text{C}$  of -28‰. Assuming seawater  $\delta^{18}\text{O}$  values between 0‰ to  
328 0.5‰ for the Irish Sea (LeGrande and Schmidt, 2006) and that marine OM  $\delta^{13}\text{C}$   
329 typically ranges from -20‰ to -30‰, the non-AOM  $\delta^{13}\text{C}/\delta^{18}\text{O}$  component may be  
330 associated with a marine water column OM signal. According to Milodowski et al.  
331 (2009), the  $\delta^{18}\text{O}$  values for MDAC in the Irish Sea could be a result of precipitation in  
332 seawater colder than at present day. However,  $^{18}\text{O}$  enrichment in MDAC at gas seeps  
333 sites is also well documented (e.g. Aloisi et al., 2000; Bohrmann et al., 1998; Chen et  
334 al., 2005), and may be due to MDAC precipitation with  $^{18}\text{O}$ -enriched water associated  
335 with decomposing deep gas hydrate (Aloisi et al., 2000; Bohrmann et al., 1998) or  
336  $^{18}\text{O}$ -enriched water transported from deep petroleum sources (Milkov et al., 2005).  
337 Thus, the potential causes of  $^{18}\text{O}$ -enrichment in the Irish Sea cannot be reconciled  
338 here and will require further investigation.

339         Accumulations of unidentified shallow gas north of the study area have been  
340 suggested previously to be of biogenic origin (Yuan et al., 1992). Gas generation  
341 within these sediments is possible, however the volume of gas generated from thin  
342 and fairly recent sediment (Belderson, 1964) is probably much lower than that  
343 observed (Clayton, 1992; Judd and Hovland, 2007). Because the area of study is  
344 dominated by sands (Belderson, 1964; Croker et al., 2005), the gas is most likely

345 sourced from the deeper subsurface. Subcropping Palaeozoic and Mesozoic rocks of  
346 the Kish Bank Basin (Naylor et al., 1993) are obvious candidates, with Carboniferous  
347 coals subjected to biogenesis to methane being of particular interest here (e.g. Flores  
348 et al., 2008; Li et al., 2008; Ulrich and Bower, 2008; cf. Moore, 2012). Alternatively,  
349 significant mixing and microbial reworking of seeping thermogenic gas in the shallow  
350 subsurface would result in a further depleted isotope signal from the original  
351 thermogenic signature and may be occurring here. Indeed, Croker et al. (2005)  
352 favoured a thermogenic gas source based on the distribution of gas accumulations in  
353 the western Irish Sea at both sandy and muddy sediment types, and due to the  
354 occurrence of most gas accumulations and features along faults (migration pathways  
355 from the deep sub-surface). Thus, the exact source of the gas remains difficult to  
356 determine at present.

357         Active water column seepage from the CFZ mounds has been documented on  
358 one other occasion at a separate feature in the CFZ, approximately 2.5 km west  
359 (53°20'30" N, 5°39'10" S) of the site described here (Croker et al., 2002). Based on  
360 surveys to date, the CFZ appears to be a site of active gas seepage.  $\delta^{13}\text{C}$  analysis has  
361 confirmed that the precipitated carbonate is MDAC and SEM-EDS has also  
362 highlighted the presence of co-precipitated pyrite. This is in agreement with previous  
363 observations (Croker et al., 2002). Sulfate reduction is also evidenced by the presence  
364 of patches of black reducing sediments at the sediment-water interface (Fig. 2D and  
365 F). AOM is therefore a significant process regulating the flux of methane from the  
366 CFZ mounds and the formation of carbonate mounds at this site. The size and  
367 thickness of the slabs shown in Fig. 2C indicate considerable seepage over geological  
368 time, and together with echosounder data, and the presence of sulfide-rich reduced  
369 sediment indicates active methane seepage from the CFZ mounds is ongoing. Marine

370 settings experiencing long-term erosion will eventually expose MDAC formed by  
371 AOM and, since carbonate-cemented sediments are more resistant to erosion than  
372 uncemented sediments, exhumed MDAC will accumulate as lag deposits in erosional  
373 environments (Paull and Ussler, 2008). The CFZ is a dynamic erosional setting with  
374 strong hydrographic conditions (e.g. Gowen and Stewart, 2005), and it is likely that  
375 the mounds formed in the shallow subsurface and have become exposed over time.  
376 The topography of these features is also likely extensively eroded post-exposure.

377 Both the character of the detrital and authigenic component suggests carbonate  
378 authigenesis within the sediment. This seems to be a common phenomenon in most of  
379 the seeps in the marine environment (e.g. Naehr et al., 2007; Pierre and Fouquet,  
380 2007; Himmler et al., 2011), since AOM is localized to the anoxic zone at some depth  
381 within the sediment (Hinrichs et al., 1999; Boetius et al., 2000). Aragonite forms in  
382 favour over calcite in settings with relatively high alkalinity and increased sulfate  
383 concentrations (Walter, 1986; Burton, 1993). In this way, in seep settings aragonite is  
384 preferentially formed closer to the sediment-water interface (Aloisi et al., 2002;  
385 Savard et al., 1996). Formation of authigenic carbonate proceeds downward from the  
386 initial sulfate-methane transition to form carbonate crust (Greinert et al., 2002; Bayon  
387 et al., 2009). As AOM proceeds, marine sulfate enclosed in the pore water is  
388 successively consumed, giving way for more extensive precipitation of calcite in the  
389 succeeding stages (e.g. Aloisi et al., 2002; Bayon et al., 2009). Dominance of  
390 aragonite over calcite in carbonates sampled (Fig. 6) implies their formation in a  
391 sulfate-rich environment, most likely shaped by seawater reflux through permeable  
392 sandy sediment (Fig. 5).

393 Nemertesia and Sabellaria are epifaunal animals, which require a solid  
394 substrate for colonisation (Whomersley et al., 2010). Sabellaria spinulosa favours a

395 sandy erosional environment but requires a hard ground in order to get established.  
396 This species was found in very high densities covering MDAC in the mid-Irish Sea  
397 (Whomersley et al., 2010) and may be an important coloniser of carbonate grounds  
398 throughout the Irish Sea. No known seep-specialist macrofauna, such as siboglinid  
399 tubeworms or thyasirid bivalves (Dando et al., 1991) were observed during video  
400 surveying. Nor were bacterial mats, which are commonly reported in active methane  
401 seep environments (e.g. Niemann et al., 2005; Bouloubassi et al., 2009). Seep-  
402 specialists such as some siboglinid tubeworms are rarely reported in shallow shelf and  
403 coastal cold seeps and are largely restricted to deep-sea active cold seep settings (Judd  
404 and Hovland, 2007). Thus they would not be expected to occur in a setting such as the  
405 CFZ seeps. However, a more comprehensive survey of the macrofaunal diversity of  
406 the mounds is needed to rule out the occurrence and activity of seep-specialists at the  
407 CFZ. It is evident that these hard grounds are of importance as a solid substrate for  
408 normal marine epifauna, allowing for diverse ecosystems to develop (Whomersley et  
409 al., 2010), as has been observed in the North Sea (Dando et al., 1991; Jensen et al.,  
410 1992).

411         The CFZ seep carbonates contain major fatty acids previously reported among  
412 sulfate-reducing bacteria implicated in AOM (Aloisi et al., 2002; Elvert et al., 2003;  
413 Niemann and Elvert, 2008). These included  $iC_{15:0}$ ,  $aiC_{15:0}$ ,  $C_{16:1\omega5c}$ ,  $C_{17:1\omega6c}$  and  
414  $cycC_{17:0}$  (Fig. 8A).  $aiC_{15:0}$ ,  $iC_{16:0}$  and  $C_{17:1}$  fatty acids, in particular for G109 (and  
415  $iC_{16:0}$  for G107) were more depleted than other fatty acids, which suggests that  
416 sulfate-reducing bacteria involved in AOM are present. However, in general measured  
417  $\delta^{13}C$  values for most fatty acids were not significantly depleted in  $^{13}C$  (Fig. 9) and  
418 suggests that methane is not a primary substrate for the dominant bacterial  
419 populations in this setting, as has been found in some other active seep settings (e.g.

420 Pancost et al., 2000; Elvert et al., 2003; Niemann et al., 2005). This is in agreement  
421 with recent work demonstrating the occurrence of C<sub>15</sub> and C<sub>17</sub> branched fatty acids in  
422 marine particulates and regional surface sediment throughout the western Irish Sea  
423 (O'Reilly et al., 2014). MAGE have previously been reported as diagnostic lipids for  
424 sulfate-reducing bacteria implicated in AOM (Pancost et al., 2001; Rütters et al.,  
425 2001). However,  $\delta^{13}\text{C}$  measurements and the widespread occurrence of MAGE in  
426 sediments and in the water column in the western Irish Sea (unpublished data)  
427 indicate that water column input is the major source of MAGE in this study. This  
428 conclusion is supported by a recent study demonstrating the occurrence of MAGE in  
429 the water column in the Southern Ocean and eastern South Atlantic Ocean  
430 (Hernandez-Sanchez et al., 2014).

431 Commonly reported archaeal lipids such as crocetane (co-eluting with  
432 phytane), pentamethyleicosane and archaeol were observed, but in low abundance  
433 (Fig. 8B). This indicates archaea are a minor contributor to overall organic matter  
434 within these hardgrounds. These lipids are frequently among the most abundant and  
435 <sup>13</sup>C-depleted at active methane seeps (Pancost et al., 2000; Aloisi et al., 2002;  
436 Niemann et al., 2005; Bouloubassi et al., 2009). In this case biomarkers diagnostic for  
437 microalgal water column input, such as sterols, phytol and C<sub>14</sub> to C<sub>22</sub> n-alkanols  
438 (Volkman et al., 1998) were dominant in all samples. This suggests that water column  
439 input derived from marine plankton, as well as benthic microalgae, is the dominant  
440 organic matter signal in the cemented sands. Considering that the CFZ zone is located  
441 in shallow shelf waters in a setting of known high primary productivity (Gowen and  
442 Stewart, 2005), a dominant input of organic matter from the water column may be  
443 expected. The significant contribution of phytoplankton and zooplankton OM to  
444 surface sediments in the western Irish Sea has recently been demonstrated (O'Reilly

445 et al., 2014). In addition, since sand comprised over half the volume of the  
446 investigated hard grounds, one may expect to have significant contribution of marine  
447 OM and a subsequent dilution of AOM evidence in settings such as this.  $\delta^{13}\text{C}$  values  
448 therefore likely reflect this major input from photosynthetic and related heterotrophic  
449 processes and may be diluting signals from microbial biomass that could be  
450 incorporating methane (Aquilina et al., 2010). It is noteworthy, however, that certain  
451 bacterial fatty acids were more depleted relative to other lipids, and compared to  
452 regional sediments (O'Reilly et al., 2014), with measured values as low as -40‰ (Fig.  
453 9), which suggests that an unknown proportion of these fatty acids may be associated  
454 with sulfate-reducing bacteria involved in AOM. Similar moderately depleted fatty  
455 acids diagnostic for sulfate-reducing bacteria were obtained by Kinnaman et al.  
456 (2010) from MDAC concretions at 10 m water depth in the Brian Seep off Santa  
457 Barbara. AOM consortium biomass and their associated lipids are spatially highly  
458 variable and typically are highest in defined locales below the sediment surface where  
459 AOM rates are highest (e.g. Elvert et al., 2003; Aquilina et al., 2010). Therefore  
460 further targeted surveys in proximity to a venting site and from subsurface MDAC  
461 may reveal the nature of the microorganisms involved in AOM at this setting. This  
462 study highlights the complex interplay at shallow active gas seeps, between microbes  
463 utilising carbon derived from marine photosynthesis, and carbon from seeping gas.

464

## 465 **6. Conclusions**

466 Bulk isotope analysis and mineralogical analysis has confirmed that the carbonate  
467 mound features at the CFZ in the Irish Sea are MDAC. The principal authigenic  
468 mineral is aragonite. Active seepage was recorded from one of the mounds, with gas  
469 plumes detected in the water column. Underwater video footage highlighted the

470 presence of sand-covered stacked and exposed carbonate pavements. The occurrences  
471 of high densities of cemented sabellarid tubes and extensive macrofaunal colonisation  
472 of carbonates indicate the CFZ mounds, like at other MDAC sites in the Irish Sea,  
473 represent an important solid substrate and habitat for local macrofauna. The common  
474 occurrence of patches of reduced sediment and the association of authigenic aragonite  
475 with framboidal pyrite indicate that AOM is taking place in shallow subsurface. In  
476 contrast to other deep sea methane seeps with widespread MDAC, lipid biomarker  
477 analysis suggests that microbial organic matter derived from methane is of minor  
478 significance in comparison to algal detrital organic matter from the water column. The  
479 co-existence of  $\delta^{13}\text{C}$ -depleted authigenic aragonite and isotopically light methane  
480 indicates a biogenic origin of the seeping gas, possibly related to Carboniferous coal  
481 deposits. However microbial reworking of deep thermogenic methane cannot be ruled  
482 out at present.

483

## 484 **Acknowledgements**

485 We thank the crew of the RV Voyager for their help and patience and the INtegrated  
486 Mapping FOr the Sustainable Development of Ireland's MARine Resource  
487 (INFOMAR), the Irish Shelf Petroleum Studies Group of the Petroleum Infrastructure  
488 Programme, the Irish Environmental Protection Agency (EPA), QUESTOR (Queens  
489 University Belfast), the Irish Council for Science, Engineering & Technology  
490 (IRCSET), the Geological Survey of Ireland (GSI) and the Science foundation of  
491 Ireland (SFI) for funding this research.

492

## 493 **References**

494 Aloisi, G., Pierre, C., Rouchy, J.-P., Foucher, J.-P., Woodside, J. and the MEDINAUT  
495 Scientific Party. 2000. Methane-related authigenic carbonates of eastern Mediterranean  
496 Sea mud volcanoes and their possible relation to gas hydrate destabilization. *Earth  
497 and Planetary Science Letters* 184, 321–338.

498 Aloisi, G., Bouloubassi I., Heijs S.K., Pancost R.D., Pierre C., Sinninghe Damsté J.S.,  
499 Gottschal J.C., Forney, L.J. 2002. CH<sub>4</sub>-consuming microorganisms and the formation  
500 of carbonate crusts at cold seeps. *Earth and Planetary Science Letters* 203, 195–203.

501 Aquilina, A., Knab, N.J., Knittel, K., Kaur, G., Geissler, J., Kelly, S.P., Fossing, H.,  
502 Boot, C.S., Parkes, R.J., Mills., R.A., Boetius, A., Lloyd, J.R., Pancost, R.D. 2010.  
503 Biomarker indicators for anaerobic oxidizers of methane in brackish marine sediments  
504 with diffusive methane fluxes. *Organic Geochemistry* 41, 414–426.

505 Bacelle, L., Bosellini, A. 1965. Diagrammi per la stima visiva della composizione  
506 percentuale nelle rocce sedimentarie. *Annali della Università di Ferrara, Sezione IX,  
507 Science Geologiche e Paleontologiche* 1, 59–62.

508 Bayon, G., Henderson, G.M., Bohn, M. 2009. U-Th stratigraphy of a cold seep  
509 carbonate crust. *Chemical Geology* 260, 47–56.

510 Beal E.J., House C.H., Orphan V.J. 2009. Manganese- and iron-dependent marine  
511 methane oxidation. *Science* 325, 184–187.

512 Belderson, R.H. 1964. Holocene sedimentation in the western half of the Irish Sea.  
513 *Marine Geology* 2, 147–163.

514 Boetius, A., Ravensschlag, K., Schubert, C.J., Rickert, D., Widdel, F., Gieseke, A.,  
515 Amann, R., Jørgensen, B.B., Witte, U., Pfannkuche, O. 2000. A marine microbial  
516 consortium apparently mediating anaerobic oxidation of methane. *Nature* 407, 623–  
517 626.

518 Bohrmann, G., Greinert, J., Suess, E., Torres, M. 1998. Authigenic carbonates from  
519 the Cascadia subduction zone and their relation to gas hydrate stability. *Geology* 26,  
520 647–650.

521 Bouloubassi, I., Nabais, E., Pancost, R.D., Lorre, A., Taphanel, M.H. 2009. First  
522 biomarker evidence for methane oxidation at cold seeps in the Southeast Atlantic  
523 (REGAB pockmark). *Deep Sea Research Part II* 56, 2239–2247.

524 Burton, E.A. 1993. Controls on marine carbonate cement mineralogy: review and  
525 reassessment. *Chemical Geology* 105, 163–179.

526 Capozzi, R., Guido, F.L., Oppo, D., Gabbianelli, G. 2012. Methane-Derived  
527 Authigenic Carbonates (MDAC) in northern-central Adriatic Sea: Relationships  
528 between reservoir and methane seepages. *Marine Geology* 332–334, 174–188.

529 Chen, D.F., Huang, Y.Y., Yuan, X.L., Cathles III, L. M. 2005. Seep carbonates and  
530 preserved methane oxidizing archaea and sulfate reducing bacteria fossils suggest  
531 recent gas venting on the seafloor in the Northeastern South China Sea. *Marine and*  
532 *Petroleum Geology* 22, 613–621.

533 Claypool, G.E., Kvenvolden, K.A. 1983. Methane and other hydrocarbon gases in  
534 marine sediment. *Annual Review of Earth Sciences* 11, 299–327.

535 Clayton, C. 1992. Source volumetrics of biogenic gas generation. In: Vially, R. (Ed.)  
536 *Bacterial Gas*. Paris, Editions Technip, 191–204.

537 Crémière, A., Pierre, C., Blanc-Valleron, M.-M., Zitter, S., Çağatay, M.N., Henry, P.  
538 2012. Methane-derived authigenic carbonates along the North Anatolian fault system  
539 in the Sea of Marmara (Turkey). *Deep-Sea Research I* 66, 114–130.

540 Croker, P.F. 1995. Shallow gas accumulation and migration in the western Irish Sea.  
541 *Geological Society of London, Special Publications* 93, 41–58.

542 Croker, P.F., O'Loughlin, O. 2001. Celtic Voyager Cruise Report – 18<sup>th</sup> –19<sup>th</sup> April,  
543 4<sup>th</sup> –6<sup>th</sup> May. Petroleum Affairs Division, Dublin, December 2001.

544 Croker, P.F., Garcia-Gil, S., Monteys, X., O'Loughlin, O. 2002. A multibeam survey  
545 of the Codling Fault Zone, western Irish Sea. Irish Geological Research Meeting,  
546 UCD, February 2002.

547 Croker, P.F., Kozachenko, M., Wheeler, A.J. 2005. Gas-related seepage features in  
548 the western Irish Sea IRL-SEA6. Tech Rep Strategic Environmental Assessment of  
549 the Irish Sea (SEA6). Petroleum Affairs Division: Dublin, Ireland.

550 Dando, P. 2010. Biological Communities at Marine Shallow-Water Vent and Seep  
551 Sites. In: Kiel, S. (Ed.). Vent and Seep Biota. Aspects from Microbes to Ecosystems,  
552 Dodrecht, Heidelberg, London, New York, Springer, p. 333–378.

553 Dando, P., Austen, M., Burke, R., Kendall, M., Kennicutt, M., Judd, A., Moore, D.C.,  
554 O'Hara, S.C.M., Schmaljohann, R., Southward, A.J. 1991. Ecology of a North Sea  
555 pockmark with an active methane seep. Marine Ecology Progress Series 70, 49–63.

556 Dobson, M., Whittington, R. 1979. The geology of the Kish Bank Basin. Journal of  
557 the Geological Society London 136, 243–249.

558 Elvert, M., Boetius, A., Knittel, K., Jørgensen, B.B. 2003. Characterization of specific  
559 membrane fatty acids as chemotaxonomic markers for sulfate-reducing bacteria  
560 involved in anaerobic oxidation of methane. Geomicrobiology Journal 20, 403–419.

561 Feng, D., Chen, D., Roberts, H.H. 2008. Sedimentary fabrics in the authigenic  
562 carbonates from Bush Hill: implication for seabed fluid flow and its dynamic  
563 signature. Geofluids 8, 301–310.

564 Feng, D., Chen, D., Peckmann, J., Bohrmann, G. 2010. Authigenic carbonates from  
565 methane seeps of the northern Congo fan: Microbial formation mechanism. Marine

566 and *Petroleum Geology* 27, 748–756.

567 Fleischer, P., Orsi, T., Richardson, M., Anderson, A. 2001. Distribution of free gas in  
568 marine sediments: a global overview. *Geo-Marine Letters* 21, 103–122.

569 Flores, R.M., Rice, C.A., Stricker, G.D., Warden, A., Ellis, M.S. 2008. Methanogenic  
570 pathways of coal-bed gas in the Powder River Basin, United States: The geologic  
571 factor. *International Journal of Coal Geology* 27, 52–75.

572 Forster, P., Ramaswamy, V., Artaxo P., Berntsen, T., Betts, R., Fahey, D.W.,  
573 Haywood, J., Lean, J., Lowe, D.C., Myhre, G., Nganga, J., Prinn, R., Raga, G.,  
574 Schulz, M., Van Dorland, R. 2007. Changes in atmospheric constituents and in  
575 radiative forcing. In: Solomon, S., Qin, D., Manning, M., Chen, Z., Marquis, M.,  
576 Averyt, K.B., Tignor, M., Miller, H.L. (Eds.). *Climate Change 2007: The physical  
577 science basis. Contribution of Working Group I to the Fourth Assessment Report of  
578 the Intergovernmental Panel on Climate Change*, Cambridge, Cambridge University  
579 Press: United Kingdom and USA, p. 129–234.

580 Gowen R.J., Stewart B. 2005. The Irish Sea: nutrient status and phytoplankton.  
581 *Journal of Sea Research* 54, 36–50.

582 Greinert, J., Bohrmann, G., Suess, E. 2001: Gas hydrate-associated carbonates and  
583 methane-venting at Hydrate Ridge: Classification, distribution and origin of  
584 authigenic lithologies. In: Paull, C.K., Dillon, P.W. (Eds.), *Natural Gas Hydrates:  
585 Occurrence, Distribution and Detection. Geophysical Monograph* 124, 99–113.

586 Greinert, J., Bohrmann, G., Elvert, M. 2002. Stromatolitic fabric of authigenic  
587 carbonate crusts: result of anaerobic methane oxidation at cold seeps in 4,850 m water  
588 depth. *International Journal Of Earth Sciences* 91, 698–711.

589 Haas A., Peckmann, J., Elvert, M., Sahling, H., Bohrmann, G. 2010. Patterns of  
590 carbonate authigenesis at the Kouilou pockmarks on the Congo deep-sea fan. *Marine*  
591 *Geology* 268, 129–136.

592 Hernandez-Sanchez, M.T., Homoky, W.B., Pancost, R.D., 2014. Occurrence of 1-O-  
593 monoalkyl glycerol ether lipids in ocean waters and sediments. *Organic Geochemistry*  
594 66, 1–13.

595 Himmler, T., Brinkmann, F., Bohrmann, G., Peckmann, J. 2011. Corrosion patterns of  
596 seep-carbonates from the eastern Mediterranean Sea. *Terra Nova* 23, 206–212.

597 Hinrichs, K.-U., Hayes, J.M., Sylva, S.P., Brewer, P.G. DeLong, E.F. 1999. Methane-  
598 consuming archaeobacteria in marine sediments. *Nature* 398, 802–805.

599 Hovland, M., Talbot, M.R., Qvale, H., Olausson, S., Aasberg, L. 1987. Methane-  
600 related carbonate cements in pockmarks of the North Sea. *Journal of Sedimentary*  
601 *Petrology* 57, 881–892.

602 Hovland, M., Gardner, J., Judd, A. 2002. The significance of pockmarks to  
603 understanding fluid flow processes and geohazards. *Geofluids* 2, 127–136.

604 Ivanov, M., Mazzini, A., Blinova, V., Kozlova, E., Laberg, J.-S., Matveeva, T.,  
605 Taviani, M., Kaskov, N. 2010. Seep mounds on the Southern Vøring Plateau. *Marine*  
606 *and Petroleum Geology* 27, 1235–1261.

607 Jackson, D.I., Jackson, A.A., Evans, D., Wingfield, R.T.R., Barnes, R.P., Arthur, M.J.  
608 1995. *The geology of the Irish Sea*. BGS UK Offshore regional Rep, HMSO, London.

609 Jensen, P., Aagaard, I., Burke, Jr R.A., Dando, P.R., Jørgensen, N.O., Kuijpers, A.,  
610 Laier, T., O'Hara, S.C.M., Schmaljohann, R. 1992. 'Bubbling reefs in the Kattegat:  
611 Submarine landscapes of carbonate-cemented rocks support a diverse ecosystem at  
612 methane seeps. *Marine Ecology Progress Series* 83, 103–112.

613 Jørgensen, N.O. 1989. Holocene methane-derived dolomite-cemented sandstone  
614 pillars from the Kattegat, Denmark. *Marine Geology* 88, 71–81.

615 Judd, A.G. 2005. Strategic Environmental Assessment of the Irish Sea (SEA6): The  
616 distribution and extent of methane-derived authigenic carbonate. Department of Trade  
617 and Industry, United Kingdom.

618 Judd, A., Croker, P., Tizzard, L., Voisey, C. 2007. Extensive methane-derived  
619 authigenic carbonates in the Irish Sea. *Geo-Marine Letters* 27, 259–267.

620 Judd, A., Hovland, M. 2007. Seabed fluid flow: the impact on geology, biology and  
621 the marine environment. Cambridge University Press: Cambridge, UK.

622 Kinnaman, F.S., Kimball, J.B., Busso, L., Birgel, D., Ding, H., Hinrichs, K.-U.,  
623 Valentine, D.L. 2010. Gas flux and occurrence at a shallow seep of thermogenic  
624 natural gas. *Geo-Marine Letters* 30, 355–365.

625 Knittel, K., Boetius, A. 2009. Anaerobic oxidation of methane: progress with an  
626 unknown process. *Annual Reviews of Microbiology* 63, 311–334.

627 Lavoie, D., Pinet, N., Duchesne, M., Bolduc, A., Larocque, R. 2010. Methane-derived  
628 authigenic carbonates from active hydrocarbon seeps of the St. Lawrence Estuary,  
629 Canada. *Marine and Petroleum Geology* 27, 1267–272.

630 Levin, L.A., James, D.W., Martin, C.M., Rathburn, A.E., Harris, L.H., Michener,  
631 R.H. 2000. Do methane seeps support distinct macrofaunal assemblages?  
632 Observations on community structure and nutrition from the northern California slope  
633 and shelf. *Marine Ecology Progress Series* 208, 21–39.

634 Levin, L.A. 2005. Ecology of cold seep sediments: interactions of fauna with flow,  
635 chemistry and microbes, in: Gibson, R.N., Atkinson, R.J.A., Gordon, A.G.M. (Eds.).  
636 *Oceanography and Marine Biology: An Annual Review* 43, 1–46.

637 Li, D., Hendry, P., Faiz, M. 2008. A survey of the microbial populations in some  
638 Australian coalbed methane reservoirs. *International Journal of Coal Geology* 27, 14–  
639 24.

640 Magalhães, V.H., Pinheiro, L.M., Ivanov, M.K., Kozlova, E., Blinova, V., Kolganova,  
641 J., Vasconcelos, C., McKenzie, J.A., Bernasconi, Kopf, A.J., Díaz-del-Río, V.,  
642 González, F.J., Somoza, L. 2012. Formation processes of methane-derived authigenic  
643 carbonates from the Gulf of Cadiz. *Sedimentary Geology* 243–244, 155–168.

644 Mah, R.A., Ward, D.M., Baresi, L., Glass, T.L. 1977. Biogenesis of methane. *Annual*  
645 *Review of Microbiology* 31, 309–341.

646 Martens, C.S., Chanton, J.P., Paull, C.K. 1991. Biogenic methane from abyssal brine  
647 seeps at the base of the Florida escarpment. *Geology* 19, 851–854.

648 Mazzini, A., Aloisi, G., Akhmanov, G.G., Parnell, J., Cronin, B.T., Murphy, P. 2005.  
649 Integrated petrographic and geochemical record of hydrocarbon seepage on the  
650 Vøring Plateau. *Journal of the Geological Society* 162, 815–827.

651 Milucka, J., Ferdelman, T.G., Polerecky, L., Franzke, D., Wegener, G., Schmid, M.,  
652 Lieberwirth, I., Wagner, M., Widdel, F., Kuypers, M.M. 2012. Zero-valent sulphur is  
653 a key intermediate in marine methane oxidation. *Nature* 491, 541–546.

654 Moore, T.A. 2012. Coalbed methane: A review. *International Journal of Coal*  
655 *Geology* 101, 36–81.

656 Naehr, T.H., Eichhubl, P., Orphan, V.J., Hovland, M., Paull, C.K., Ussler III, W.,  
657 Lorenson, T.D. & Greene, H.G. 2007. Authigenic carbonate formation at hydrocarbon  
658 seeps in continental margin sediments: a comparative study. *Deep-Sea Research II*,  
659 54, 1268–1291.

660 Naylor, D., Haughey, N., Clayton, G., Graham, J.R. 1993. The Kish Bank Basin,  
661 offshore Ireland. In: Parker, J.R. (Ed.). *Petroleum Geology of Northwest Europe:*  
662 *Proceedings of the 4th Conference. Petroleum Geology Conference series 4, 845–855.*

663 Nichols, P.D., Guckert, J.B., White, D.C. 1986. Determination of monosaturated fatty  
664 acid double-bond position and geometry for microbial monocultures and complex  
665 consortia by capillary GC-MS of their dimethyl disulphide adducts. *Journal of*  
666 *Microbiological Methods* 5, 49–55.

667 Niemann, H., Elvert, M., Hovland, M., Orcutt, B., Judd, A., Suck, I., Gutt, J., Joye, S.,  
668 Damm, E., Finster, K., Boetius, A. 2005. Methane emission and consumption at a  
669 North Sea gas seep (Tommeliten area). *Biogeosciences Discussions* 2, 1197–1241.

670 Niemann, H., Elvert, M. 2008. Diagnostic lipid biomarker and stable carbon isotope  
671 signatures of microbial communities mediating the anaerobic oxidation of methane  
672 with sulphate. *Organic Geochemistry* 39, 1668–1677.

673 Olu-Le Roy, K., Sibuet, M., Fiala-Medioni, A., Gofas, S., Salas, C., Mariotti, A.,  
674 Foucher, J.P., Woodside, J. 2004. Cold seep communities in the deep eastern  
675 Mediterranean Sea: composition, symbiosis and spatial distribution on mud  
676 volcanoes. *Deep-Sea Research I* 51, 1915–1936.

677 O'Reilly, S.S., Murphy, S., Coleman, N., Monteys, X., Szpak, M., O'Dwyer, T.,  
678 Kelleher, B.P. 2012. Chemical and physical features of living and non-living maerl  
679 rhodoliths. *Aquatic Biology* 15, 215–224.

680 O'Reilly, S.S., Szpak, M.T., Flanagan, P.V., Monteys, X., Murphy, B.T., Jordan, S.F.,  
681 Allen, C.C.R., Simpson, A.J., Mulligan, S.M., Sandron, S., Kelleher, B.P. 2014.  
682 Biomarkers reveal the effects of hydrography on the sources and fate of marine and

683 terrestrial organic matter in the western Irish Sea. *Estuarine, Coastal and Shelf*  
684 *Science* 136, 157–171.

685 Pancost, R.D., Sinninghe Damste, J.S., de Lint, S., van der Maarel, M.J., Gottschal,  
686 J.C. 2000. Biomarker evidence for widespread anaerobic methane oxidation in  
687 Mediterranean sediments by a consortium of methanogenic archaea and bacteria. The  
688 Medinaut Shipboard Scientific Party. *Applied and Environmental Microbiology* 66,  
689 1126–1132.

690 Pancost, R.D., Bouloubassi, I., Aloisi, G., Sinninghe Damsté, J.S. 2001. Three series  
691 of non-isoprenoidal dialkyl glycerol diethers in cold-seep carbonate crusts. *Organic*  
692 *Geochemistry* 32, 695–707.

693 Paull, C.K., Ussler III, W., Peltzer, E.T., Brewer, P.G., Keaten, R., Mitts, P.J., Nealon,  
694 J.W., Greinert, J., Herguera, J.C., Perez, M.E. 2007. Authigenic carbon entombed in  
695 methane-soaked sediments from the northeastern transform margin of the Guayamas  
696 Basin, Gulf of California. *Deep-Sea Research II*, 54, 1240-1267.

697 Paull, C.K., Ussler III, W, 2008. Re-evaluating the significance of seafloor  
698 accumulations of methane-derived carbonates: seepage or erosion indicators?  
699 *Proceedings of the 6th International Conference on Gas Hydrates, Vancouver,*  
700 *Canada.*

701 Peckmann J., Reimer A., Luth U., Luth C., Hansen B.T., Heinicke C., Hoefs, J.  
702 Reitner, J. 2001. Methane-derived carbonates and authigenic pyrite from the  
703 northwestern Black Sea. *Marine Geology* 177, 129–150.

704 Peckmann, J., Thiel, V. 2004. Carbon cycling at ancient methane seeps.  
705 *Chemical Geology* 205, 443–467.

706 Pierre, C., Fouquet, Y. 2007. Authigenic carbonates from methane seeps of the Congo  
707 deep-sea fan. *Geo-Marine Letters* 27, 249–257.

708 Rathburn, A.E., Levin, L.A., Held, Z., Lohmann, K.C. 2000. Benthic foraminifera  
709 associated with cold methane seeps on the northern California margin: ecology and  
710 stable isotope composition. *Marine Micropaleontology* 28, 247–266.

711 Reitner, J., Peckmann, J., Reimer, A., Schumann, G., Theil, V. 2005. Methane-  
712 derived carbonate build-ups and associated microbial communities at cold seeps on  
713 the lower Crimean shelf (Black Sea). *Facies* 51, 66–79.

714 Ritger, S., Carson, B., Suess, E. 1987. Methane-derived authigenic carbonates formed  
715 by subduction-induced pore-water expulsion along the Oregon/Washington margin.  
716 *Geological Society of America Bulletin* 98, 147–156.

717 Rütters, H., Sass, H., Cypionka, H., Rullkötter, J. 2001. Monoalkylether  
718 phospholipids in the sulfate-reducing bacteria *Desulfosarcina variabilis* and  
719 *Desulforhabdus amnigenus*. *Archives of Microbiology* 176, 435–442.

720 Sackett, W.M. 1978. Carbon and hydrogen isotope effects during the thermocatalytic  
721 production of hydrocarbons in laboratory simulation experiments. *Geochemica et*  
722 *Cosmochemica Acta* 42, 571–580.

723 Sahling, H., Galkin, S.V., Salyuk, A., Greinert, J., Foerstel, H., Piepenburg, D., Suess,  
724 E. 2003. Depth-related structure and ecological significance of cold-seep  
725 communities-a case study from the Sea of Okhotsk. *Deep Sea Research I* 50, 1391–  
726 1409.

727 Savard, M.M., Beauchamp, B., Veizer, J. 1996. Significance of aragonite cements  
728 around Cretaceous marine methane seep. *Journal of Sedimentary Research* 66, 430–  
729 438.

730 Schmidt, M., Botz, R., Winn, K., Stoffers, P., Thiessen, O., Herzig, P. 2002. Seeping  
731 hydrocarbons and related carbonate mineralization in sediments south of Lihir Island  
732 (New Ireland fore arc basin, Papua New Guinea). *Chemical Geology* 186, 249–264.

733 Schoell, M. 1988. Multiple origins of methane in the Earth. *Chemical Geology* 71, 1–  
734 10.

735 Sibuet, M., Olu, K. 1998. Biogeography, biodiversity and fluid dependence of deep-  
736 sea cold-seep communities at active and passive margins. *Deep-Sea Research II* 45,  
737 517–567.

738 Stakes, D.S., Orange, D., paduan, J.B., Salamy, K.A., Maher, N. 1999. Cold seeps and  
739 authigenic carbonate formation in Monterey Bay, California. *Marine Geology* 159,  
740 93–109.

741 Svensen, H., Planke, S., Sørenssen, A.-M., Jamtveit, B., Myklebust, R., Eidem, T.R.,  
742 Rey, S.S. 2004. Release of methane from a volcanic basin as a mechanism for initial  
743 Eocene global warming. *Nature* 429, 542–545.

744 Tsunogai, U., Yoshida, N., Gamo, T. 2002. Carbon isotopic evidence of methane  
745 oxidation through sulfate reduction in sediment beneath cold seep vents on the  
746 seafloor at Nankai Trough. *Marine Geology* 187, 145–160.

747 Ulrich, G., Bower, S. 2008. Active methanogenesis and acetate utilization in Powder  
748 River Basin coals, United States. *International Journal of Coal Geology* 76, 25–33.

749 Valentine, D.L., Reeburgh, W.S. 2000. New perspectives on anaerobic methane  
750 oxidation. *Environmental Microbiology* 2, 477–484.

751 van Dover, C.L., Aharon, P., Bernhard, J.M., Caylor, E., Doerries, M., Flickinger, W.,  
752 Gilhooly, W., Goffredi, S.K., Knick, K.E., Macko, S.A., Rapaport, S., Raufels, E.C.,  
753 Ruppel, C., Salerno, J.L., Seitz, R.D., Sen Gupta, B.K., Shank, T., Turnipseed,

754 M., Vrijenhoek, R. 2003. Blake Ridge methane seeps: characterization of a soft-  
755 sediment, chemosynthetically based ecosystem. *Deep-Sea Research I* 50, 281–230.

756 Volkman, J.K., Barrett, S.M., Blackburn, S.I., Mansour, M.P., Sikes, E.L., Gelin, F.  
757 1998. Microalgal biomarkers: A review of recent research developments. *Organic*  
758 *Geochemistry* 29, 1163–1179.

759 von Rad, U., Rösch, H., Berner, U., Geyh, M., Marchig, V., Schulz, H. 1996.  
760 Authigenic carbonates derived from oxidized methane vented from the Makran  
761 accretionary prism off Pakistan. *Marine Geology* 136, 55–77.

762 Walter, L.M. 1986. Relative efficiency of carbonate dissolution and precipitation  
763 during diagenesis: a progress report on the role of solution chemistry. In: Gauties,  
764 D.L. (Ed.), *Roles of organic matter in mineral diagenesis*, SEPM (Society for  
765 *Sedimentary Geology*) Special Publication 38, 1–12.

766 Whiticar, M.J. 1999. Carbon and hydrogen isotope systematics of bacterial formation  
767 and oxidation of methane. *Chemical Geology* 161, 291–314.

768 Whomersley, P., Wilson, C., Clements, A., Brown, C., Long, D., Leslie, A.,  
769 Limpenny, D. 2010. Understanding the marine environment - seabed habitat  
770 investigation of submarine structures in the mid Irish Sea and Solan Bank Area of  
771 Search (AoS). JNCC Report No. 430.

772 Yuan, F., Bennell, J., Davis, A. 1992. Acoustic and physical characteristics of gassy  
773 sediments in the western Irish Sea. *Continental Shelf Research* 12, 1121–1134.

774 **Tables and Figures**

775 Table 1. Summary data of collected cemented carbonates from the Codling Fault Zone.  
776

777 Table. 2. Carbon and oxygen stable isotope composition of the carbonate sample PMO 217.327-109  
778 from site G109 (relative to Vienna Pee Dee Belemnite).

779

780 Fig. 1. The Codling Fault Zone mound features (white arrows), sampling stations (white crosses),  
781 underwater video tracklines (dark grey lines), and captured image stills of exposed carbonates or black  
782 reduced sediment (white stars). A. Location of the area of study. B. A 3D Fledermaus image showing  
783 the topography of some of the mounds features.

784

785 Fig. 2. Underwater towed video (A to F) and grab sampling (G to I) of Codling Fault mound targets. A.  
786 Semi-exposed nodules and pavement (P1). B. Semi-exposed hardgrounds (P2). C. Pavement stacking  
787 (P3). D. Reduced surface sediment (P4). E. Large exposed hardgrounds (P5). F. Exposed colonised and  
788 non-colonised hardgrounds (P6). G. G103. H. G107. I. G109, a hardground colonised by a Nemertesia  
789 hydroid. Unlabelled scale bars = 25cm. The locations for underwater still images and sampling stations  
790 are given in Fig. 1 and Table 1.

791

792 Fig. 3. Single beam echosounder profile showing topography of mound features and active gas seepage  
793 to the water column from close to its apex. The location of the mound is shown in Fig. 1.

794

795 Fig. 4. A, B. Representative SEM-EDS analyses of the composition of sampled hard grounds. C. SEM  
796 micrograph showing carbonate-cemented quartz grain. D. Aragonite crystals and framboidal pyrite. E.  
797 Detail of framboidal pyrite.

798

799 Fig. 5. Aragonite cemented allochemic sandstone with bioclasts (G109). All microphotographs from  
800 PMO 217.327. A. Low magnification view of petrographic thin section; transmitted light. Note the  
801 large contribution of quartz grains in the rock volume. Empty cavities visible in the lower part of the  
802 picture are a product of sample preparation. B Detail showing a possible glaucony granule (black  
803 arrow) and an echinoderm skeletal fragment (grey arrow). C. Detail showing a bivalve fragment,  
804 possibly an oyster (black arrow), and a red algal fragment (grey arrow). D. Detail showing a balanid  
805 barnacle fragment (black arrow). E. Detail showing a gastropod (black arrow) and a possible  
806 foraminiferan (grey arrow). F. Same area as in E in polarized light.

807

808 Fig. 6. X-ray powder diffractogram of sample PMO 217.327. The blue rhombi represent quartz, red  
809 squares represent aragonite and red triangles represent Mg-calcite.

810

811 Fig. 7. Crossplot of carbon and oxygen stable isotope data from sample PMO 217.327, with data from  
812 Milodowski et al., (2009).

813

814 Fig. 8. Total ion chromatograms of a representative phospholipid fatty acid sample (A) and an alcohol  
815 fraction (B) from extracted aragonite-cemented quartz (G109 and G. Major compounds are labeled.

816 Fatty acid nomenclature is according to X:Y $\omega$ Z, where X refers to the number of carbon atoms present,

817 Y refers to the number of double bonds on the carbon chain and Z refers to the position of the first

818 double bond from the methyl end. Sterol nomenclature is according to C<sub>x</sub> $\Delta^y$  where Y refers to the

819 position of double bond(s) on the sterol skeleton.

820

821 Fig. 9. Measured  $\delta^{13}\text{C}$  values for selected biomarkers extracted from samples G103, G107 and G109.

822 See Fig. 1. for station location. IS = internal standard (5 $\alpha$ -cholestane).

823